HHS Public Access

Author manuscript

Photochem Photobiol. Author manuscript; available in PMC 2016 November 01.

Published in final edited form as:

Photochem Photobiol. 2015 November ; 91(6): 1469–1478. doi:10.1111/php.12503.

Noninvasive Optical Imaging of UV-Induced Squamous Cell Carcinoma in Murine Skin: Studies of Early Tumor Development and Vitamin D Enhancement of Protoporphyrin IX Production

Kishore R. Rollakanti[a,b], **Sanjay Anand**[b,c], **Scott C. Davis**[d], **Brian W. Pogue**[d], and **Edward V. Maytin**[a,b,c,*]

[a]Department of Chemical and Biomedical Engineering, Cleveland State University, 2121 Euclid Avenue, Cleveland, OH, USA 44115

[b]Department of Biomedical Engineering, Cleveland Clinic, 9500 Euclid Avenue, Cleveland, OH, USA 44195

[c]Department of Dermatology, Cleveland Clinic, 9500 Euclid Avenue, Cleveland, OH, USA 44195

[d]Thayer School of Engineering, Dartmouth College, 8000 Cummings Hall, Hanover, NH, USA 03755

Abstract

Better noninvasive techniques are needed to monitor protoporphyrin IX (PpIX) levels before and during photodynamic therapy (PDT) of squamous cell carcinoma (SCC) of the skin. Our aim was to evaluate: (1) multispectral fluorescent imaging of ultraviolet light (UV)-induced cancer and precancer in a mouse model of SCC; (2) multispectral imaging and probe-based fluorescence detection as a tool to study Vitamin D (VD) effects on aminolevulinic acid (ALA)-induced PpIX synthesis. Dorsal skin of hairless mice was imaged weekly during a 24-week UV carcinogenesis protocol. Hot spots of PpIX fluorescence were detectable by multispectral imaging beginning at 14 weeks of UV exposure. Many hot spots disappeared after cessation of UV at week 20, but others persisted or became visible after week 20, and corresponded to tumors that eventually became visible by eye. In SCC-bearing mice pretreated with topical VD before ALA application, our optical techniques confirmed that VD preconditioning induces a tumor-selective increase in PpIX levels. Fluorescence-based optical imaging of PpIX is a promising tool for detecting early SCC lesions of the skin. Pretreatment with VD can increase the ability to detect early tumors, providing a potential new way to improve efficacy of ALA-PDT.

INTRODUCTION

Squamous cell carcinoma (SCC) of the skin is a very common cancer (250,000 new cases/year in the United States, second only to basal cell carcinoma) and typically occurs in Caucasian patients as a result of chronic sun exposure; papillomaviruses and immunosuppression play additional etiological roles (1–5). SCC tumors develop from UV- or chemically-damaged epidermal keratinocytes, which undergo neoplastic progression from

Corresponding author: maytine@ccf.org (Edward V. Maytin).

early precursor lesions called *actinic keratoses* (*AK*), to fully-developed SCC tumors. In humans, AK lesions comprise rough, red scaly patches on the face, scalp forearms, hands, and other sun-exposed regions. It is very important to treat these lesions to prevent progression to SCC, as the latter can invade and metastasize (1, 2).

Currently, the most popular therapy for AK is cryosurgery, i.e., freezing with liquid nitrogen, which is very effective locally but carries the disadvantage that lesions must be visualized by the physician. UV-induced neoplastic changes typically begin at a microscopic level, with neoplastic cells distributed over widespread areas of sun-damaged skin (an effect called *field cancerization*) (6). Physicians treating with liquid nitrogen often miss many precancers because they cannot see them, and later on, visible AK lesions appear in the untreated locations. Therefore, two related challenges can be identified regarding AK/SCC detection and management. One challenge is to find a way to detect SCC precursors as early as possible; the other is to develop better methods for treating all pre-SCC lesions in a field cancerization setting, in addition to dealing with the more advanced lesions. Accordingly, the first goal of our study was to examine the utility of a noninvasive optical method for detecting SCC precursors at an early stage. The second was to use that method to evaluate a new type of AK/SCC treatment that involves light.

Regarding the second goal, the treatment we wished to assess with our noinvasive optical technique was Photodynamic Therapy (PDT), a modality specifically designed for treating AK in broad areas of field cancerization. To perform PDT, a topical formulation of aminolevulinic acid (ALA) (7, 8) or methyl-aminolevulinate (MAL)(9, 10) is applied to the desired area of skin, and allowed to incubate (typically for 1 to 4 hours) prior to illumination with strong visible light. ALA or MAL is taken up by tumor cells and converted into the actual photosensitizing molecule, protoporphyrin IX (PpIX) (11). Importantly, PpIX is preferentially synthesized and retained in tumor cells, relative to normal skin, so that when PpIX is activated by light, cytotoxic reactive oxygen species are generated and the tumor cells are destroyed, with sparing of normal tissues (11, 12). Unfortunately, the efficacy of PDT is sometimes suboptimal. For AK, clearance rates are never 100% and sometimes only ~50%, especially on difficult areas such as the chronically photodamaged scalp of bald men (13). When used to treat full-fledged SCC tumors (as is often done in Europe), PDT treatment responses are very good for superficial SCC, but for thicker SCC the recurrence rates after 12–36 months are unacceptably high (24–60%) as compared to <10% recurrences after surgery (13, 14). However, although a single PDT session is seldom a definitive cure, multiple PDT sessions do have an important role for shrinking large SCC prior to definitive excision, and for managing SCC in patients for whom scarring and fibrosis might severely compromise function. In this regard, PDT has an important advantage that cannot be overstated, i.e., PDT-treated areas heal without a scar (and in fact PDT may have anti-fibrotic properties) (15, 16).

About a decade ago, in an attempt to find ways to increase PDT efficacy and thereby expand its usefulness, our laboratory embarked on a program to identify agents that could be combined with PDT to boost the accumulation of intratumoral PpIX, by increasing the activity of the mitochondrial heme synthesis pathway; reviewed by Anand *et al.* in (17). In preclinical mouse models and more recently in human patients, we have shown that

preconditioning of tumors with certain protoporphyrin-enhancing agents, including methotrexate (18, 19), 5-Fluorouracil (20) and Vitamin D (VD) (21–24), markedly increases not only the tumor-specific accumulation of PpIX, but also the cytotoxic treatment effect once illumination is applied. Our previous studies employed skin biopsies and tumor sectioning to assess PpIX levels by biochemical and confocal fluorescence techniques. For future studies, however, a noninvasive technique for evaluating the PpIX-enhancing ability of combination agents *in vivo*, without requiring a biopsy, would be very valuable to have.

In the current study, we describe a sensitive, noninvasive optical method for imaging PpIX fluorescence, and show that the technique is capable of detecting very small cutaneous SCC tumors. This was accomplished using a commercially available *in vivo* imaging system, Maestro EX IVIS®, for detection of PpIX fluorescence in neoplastic skin regions following ALA application. For validation, we used a probe based fluorescence dosimetry system developed in-house. Both of these optical systems were applied to a murine model of UV carcinogenesis, in order to: (i) demonstrate an ability to detect small SCC tumors at a very early stage of development, and (ii) noninvasively analyze the ability of VD preconditioning to enhance tumor-selective accumulation of PpIX in SCC tumors in living mice.

MATERIALS & METHODS

Reagents

Aquaphor® healing ointment, and Vectical™ (1α, 25-dihydroxyvitamin D_3, calcitriol, VD) ointment 3 mcg/g, were purchased from Beiersdorf, Inc. (Wilton, CT) and Galderma Laboratories, L.P. (Fort Worth, TX), respectively. Levulan® solution (20% aminolevulinic acid, in Kerastick® applicator) was purchased from DUSA Pharmaceuticals, Inc. (Wilmington, MA). Isoflurane (1-chloro-2,2,2-trifluoroethyl difluoromethyl ether, Piramal Critical Care, Inc. Bethlehem, PA) was obtained from the hospital pharmacy of the Cleveland Clinic, Cleveland, OH.

UV induced AK/SCC mouse model

To create an AK/SCC model, the dorsal side of SKH-1 hairless male and female mice at 8 weeks of age was UV-irradiated three times weekly, using a UV apparatus (Fig. 1a) as previously described by Agarwal et al. (25, 26) with few modifications. The spectral irradiance of the ultraviolet lamps was 280–400 nm, providing 80% UV-B and 20% UV-A. Starting from week 1, UV exposure was initiated at 90 mJ/cm^2 per session, and the dose was increased by 10% per week until it reached a maximum of 175 mJ/cm^2, after which the dose was maintained at 175 mJ/cm^2 until week 20. Due to this chronic UV exposure, lesions of early SCC, which resemble actinic keratoses (AKs), began to appear on the dorsal skin of the mice around week 15 and many of these developed into multiple nodular and hyperplastic lesions (1–5 mm in diameter; Fig 1b) by week 20. Histological examination (Fig. 1c) showed large and thick (>100 mm^3) superficial tumors simulating papillomatosis-like human SCC pathology, which could continue to grow aggressively if left untreated (27).

Aquaphor, VD, and ALA treatment

To estimate the effectiveness of VD for enhancing PpIX synthesis, visible SCC lesions were identified on UV exposed SKH-1 mice, and a thin layer of Aquaphor® ointment (vehicle control) or Vectical® ointment (VD; 3 μg/g) was applied to the lesions using a cotton swab, once daily for three consecutive days. On the fourth day, Levulan® was applied to the tumors, and 4 h later mice were used for non-invasive analysis of PpIX using either a CCD based Maestro EX® imaging system, or a spectrometer-based probe dosimeter system (see below for full description of these devices).

In vivo imaging of PpIX using Maestro EX IVIS®

A Maestro EX multispectral *in vivo* fluorescence imaging system (Perkin-Elmer, Waltham, MA) was used to map the distribution of PpIX on SCC mice after 4 h of ALA application. This system works on the principle of exciting fluorescent molecules at a fixed excitation wavelength and recording the intensity of the emitted fluorescence over a range of wavelengths. Mice were placed in the light-tight camera box with continuous exposure to anesthesia (isoflurane, 1–3%) from nose cones on the imaging platform. Excitation was accomplished with blue light (435 to 480 nm, centered on the 455 nm peak) and fluorescence images were obtained using an emission filter, 490 nm long pass, in 10 nm steps from 500 to 720 nm. Two images were obtained, the first before Levulan® application, and the second at 4 h post-application. The image obtained before applying ALA was used to subtract the autofluorescence present in SCC tumors at 4 h post-Levulan® application, and thereby to obtain the PpIX specific fluorescence (see Fig 2a). Spectral processing (i.e., unmixing) and quantification of PpIX fluorescence was done as per the manufacturer's established protocols using Maestro EX 3.0 Image Processing software.

In vivo quantification of PpIX using a fluorescence dosimeter system

The probe-based dosimeter system consisted of two laser sources for illumination, a spectrophotometer to detect fluorescence, and optical fibers for light transmission. A schematic representation of the instrument is shown in Fig. 3a. The illumination sources were temperature controlled laser diodes emitting at 405 nm and 639 nm, respectively (World Star Tech Inc., Toronto, Ontario) and were used to excite PpIX in the Soret band and one of the Q-bands, respectively. The laser light was directed to the mouse skin through a bifurcated optical fiber probe (BIF200-UV-VIS, Ocean Optics Inc., Dunedin, FL), consisting of seven 200 μm fiber bundles (indicated in grey), with each bundle comprised of a central fiber (indicated in white) for excitation, and six collection fibers (indicated in black) to gather the fluorescence, as shown in Fig. 3b. During measurements, the probe was held in contact with the skin, the excitation light (405 or 639 nm) was delivered via the central fibers, and the remitted light was returned via the collection fibers, through a motorized six-position filter wheel (FW102C, ThorLabs Inc., Newtown, NJ) and into a spectrometer with spectral range between 200 and 1100 nm (QE65000, Ocean Optics Inc., Dunedin, FL). All control connections were consolidated in a powered USB hub connected to a laptop running a simple software interface written in LabVIEW (National Instruments, Austin, TX) which operated the system. The fluorescence signal from the tissue was normalized to a separate transmittance measurement of the incident light, to account for

variations in tissue optical properties. For use as a dosimeter, the instrument was calibrated using gelatin phantoms containing defined concentrations of PpIX. A similar version of this device has been described previously (28).

Ex vivo analysis of intracellular PpIX

After 4 h of Levulan application and in vivo investigation of PpIX, the mice were sacrificed, tumors harvested, and the tissue embedded in O.C.T. medium (Tissue-Tek; Sakura-Finetek) for frozen sectioning. PpIX-specific fluorescence (λ_{ex} 633 nm; λ_{em} 650–780 nm) from 10 μm thick cryosections was observed by confocal microscopy (Leica Microsystems, Buffalo Grove, IL) and quantified using IPLab image processing software (Signal Analytics, Vienna, VA) as previously described (19). Regions of interest (ROI), representative of the whole image, were cropped from each image and the levels of PpIX were analyzed by setting the background signal threshold such that only the fluorescence from PpIX was apparent. These PpIX-specific levels were expressed as arbitrary fluorescence units (total pixels per ROI) and the values reported relative to vehicle control.

Statistical Analysis

Numerical data were expressed as mean ± SEM. A two-sample t-test (Two-way ANOVA) was used to test the statistical significance in multiple comparisons. P-values ≤ 0.05 were considered statistically significant.

RESULTS

Maestro EX IVIS® enables non-invasive mapping of PpIX on mice with AK/SCC

Using the Maestro EX IVIS® device, two different types of measurements (image cubes) were obtained on any given day, namely, an *autofluorescence spectrum* obtained from control mice (no UV, no ALA) and a *mixed spectrum* (autofluorescence plus PpIX) from AK/SCC mice (4 h post ALA), respectively. As shown in Fig. 2a, Maestro EX 3.0 software allowed us to compute the pure PpIX spectrum (emission peak at ~640 nm, Fig. 2a) by subtracting the correct amount of autofluorescence from the mixed spectrum (autofluorescence plus PpIX).

Fig. 2b and 2c represent a brightfield image and original image cube obtained from a UV-exposed AK/SCC mouse, respectively, using the blue filter set (λ_{ex}: 455 nm and λ_{em}: 490–720 nm). The computed PpIX spectrum and autofluorescence spectra were used to separate the corresponding signals in the image cube. Images representing each of the pure signals (autofluorescence and PpIX) are shown in Fig. 2d and 2e respectively. Some of the bright spots in Fig. 2e, indicating high PpIX levels, correlate very well with the AK lesions or SCC tumors that are visible in the brightfield image (Fig. 2b). Other small grainy bright spots in Fig. 2e do not match with any visible tumors (Fig. 2b), leading us to hypothesize that some of these might represent nascent tumors that are not yet macroscopically visible.

To demonstrate the quantitative ability of optical imaging to map ALA induced PpIX production, we analyzed different regions of skin on the UV irradiated mice (Fig. 2f) for image signal intensity (Fig. 2g). Region 1, an area of skin that was lesion-free gave the

lowest signal. Regions 2 and 3, the bright yellow-to-orange areas, represent AK/SCC lesions that are also visible in the brightfield image (Fig. 2b). Region 4, the brightest area, contains not only a visible tumor but also signs of inflammation and erythema (redness) in the brightfield image. The highest density of AK/SCC lesions was generally located over the spine, suggesting that a normal angle of incident UV light at the midline (versus a more acute angle on the flanks) plays some role in absorbed UV intensity; the intensity of fluorescence light detectable by the Maestro may also be affected somewhat by the angle to the perpendicular, but we have not explored this experimentally. Overall, the data characterize an ability of this imaging method to differentiate normal skin from neoplastic regions (those with visible lesions), and from preneoplastic or inflamed regions.

A fluorescence dosimeter system differentiates AK/SCC lesions from normal skin in UV irradiated mice

A custom-built fluorescence dosimeter (shown in Fig. 3a), which makes point measurements of PpIX fluorescence in the skin, was used to estimate the difference between normal skin and AK and SCC lesions. At 4 h post ALA application, fluorescence measurements from visibly obvious AK lesions, and from normal skin that only received minimal exposure to UV (Fig. 3c) showed a statistically significant difference (Fig. 3d). The regions of interest (ROIs) on the mouse shown in Fig. 3c, illustrates how the probe dosimeter is able to distinguish areas with features similar to those already descried in Fig. 2 for the Maestro system. Thus, ROI-1 is a lesion-free area of normal skin, ROI-2 contains AK/SCC lesions without inflammation, and ROI-3 is a visible AK/SCC lesions with erythema (inflammation). The quantitative data in Fig. 3d illustrate how the probe dosimeter can discriminate between AK/SCC and normal skin (~2-fold higher signal in the former), and between inflamed vs. non-inflammed areas (e.g., a 2-fold higher signal is found in regions of inflamed vs. noninflamed AK/SCC).

Optical imaging method to follow the development of AK/SCC in UV-irradiated skin

The PpIX fluorescence detection capability of Maestro EX IVIS® was used to monitor the response of SKH-1 mouse skin to UV irradiation, both during a 20-week exposure period and in the 4 weeks after stopping UV. The camera-based imaging system allowed us to map the relative levels of PpIX at all locations on the back of each mouse, without any prior knowledge about where neoplastic lesions would ultimately develop. Fig. 4a shows examples of PpIX fluorescence images obtained 4 h post ALA application, illustrating how photon counts increased continuously until week 20, and then decreased rapidly after stopping UV irradiation. Quantification of such images also demonstrates that the area on these mice emitting photons above a set threshold level (>0.05 counts/s) was maximal at week 20, and then dropped by 80% over the next 2 weeks, presumably due to a reduction of UV-induced inflammation and hyperproliferation (Fig. 4b).

Fluorescence images from the Maestro EX IVIS® were further explored to determine their applicability for detecting AK/SCC lesions, especially early areas of neoplasia not yet visible with the naked eye. The images in Fig. 4c represent brightfield (upper panels) and IVIS PpIX fluorescence images (lower panels) from the lower back of a mouse that was monitored from weeks 14 to 24. After stopping the UV irradiation at week 20, the broad

inflammatory regions started to recede, and the number of clearly defined bright spots (high photon counts/s) increased from week 21 to week 24 (Fig. 4c, enlargement). Quantification of the speckles identified in IVIS fluorescence images, compared with AK/SCC tumors detectable in brightfield images, is shown in line plots in Fig. 4d-h obtained from five individual mice. A critical threshold size of 75 pixels was used to define the fluorescent speckle as an AK lesion (<75 pixels; triangles) or inflammatory region (>75 pixels; circles). Lesions with a 3-dimensional appearance in the photographs, confirmed by palpation on the mouse for verification, were defined as visible AK lesions in brightfield images (squares). In all the graphs, more AK lesions were detectable from the IVIS images (triangles) than from the brightfield images (squares), and both increased gradually from week 20 to 24. By comparison, the number of inflammatory regions detected on the IVIS images (circles) decreased after termination of UV irradiation. Fig. 4i shows a summary of the AK data from all mice, confirming that a significantly higher (2–3 fold) number of AK can be identified using the fluorescent imaging technique than by visual inspection alone.

Investigation of the effect of VD on PpIX synthesis using Maestro EX IVIS® imaging in vivo

After exposing a cohort of mice to UV irradiation for 20 weeks and allowing tumors to develop for an additional 5 weeks, eight mice (4 per treatment group) were chosen to test the effect of VD preconditioning on PpIX synthesis, as compared to ALA treatment alone (Fig. 5). Control mice, which had no VD preconditioning, received Aquaphor (Aq) instead. Representative brightfield images of the mice are shown in Fig. 5a and 5e. On day 1, all mice received an initial ALA treatment (4 hr incubation) for Maestro imaging, to record baseline PpIX production in the skin. From day 5 to day 7, one set of mice received Aq (vehicle) daily and the other set received topical VD daily for 3 days. On day 8, ALA was applied (4 h) and PpIX measured using the Maestro EX IVIS® imager. Data were recorded in two ways: as the area of skin emitting signal above a set threshold of 0.06 average scaled counts per second (Fig. 5d and 5h, first two bars), and as the corresponding total PpIX signal detected within those areas (Fig. 5d and 5h, bars 3 and 4). From Fig. 5b and 5c, it is apparent that pretreatment with the vehicle control had no significant effect on PpIX synthesis. The small increase in signal observed between the two ALA applications (which were spaced 8 days apart) might be due to an increase in tumor cell population, but this increase was insignificant. In comparison, a large and significant increase in PpIX signal intensity was seen in the VD preconditioned tumors (Fig. 5f and 5g). Quantification in Fig. 5h documented a 2-fold increase in signal area (i.e., relative number of tumor cells producing PpIX, Fig. 5h bars 1 and 2) and total photon counts (i.e., relative concentration of PpIX per cell, bars 3 and 4).

Use of a fluorescence dosimeter to detect tumor specific effects of VD on PpIX synthesis

An important question is whether VD enhancement in PpIX production occurs only in preneoplastic/neoplastic (AK/SCC) cells, or whether VD may also lead to increased PpIX in normal tissue. Our earlier studies in SCC in mice had indicated that normal skin is not signficantly affected by VD (21); however, that work was performed on frozen sections of subcutaneous A431 tumors, and might not be comparable to surface tumors that are of interest here. In other studies, we used a forerunner to the dosimeter described in this paper to measure PpIX noninvasively in human AK lesions; that study showed that PpIX levels

are typically higher in AK lesions than in surrounding skin, but the effects of VD were not assessed (6). Therefore, in the current study we wished to use the probe dosimeter to examine the tumor-specificity (neoplastic vs. normal) of VD effects in the skin.

In the experiment shown in Fig. 6, control mice that received no UV irradiation (Fig. 6a), and mice with visible tumors after a 24-week UV carcinogenesis protocol (Fig. 6b), were pretreated topically with vehicle (Aq) or with Vitamin D ointment (VD), daily for 3 days. On the 4th day, topical ALA was applied, and PpIX fluorescence measurements were acquired pre- and 4 h post-ALA application using 639 nm excitation light source (red channel) and a 650 nm long pass emission filter. The PpIX fluorescence measurements (post-ALA minus pre-ALA) were then compared to evaluate PpIX production under different treatment conditions. Fig. 6c shows that in normal skin, no statistically significant difference in PpIX levels was identified between vehicle (Aq) or VD preconditioned normal tissue (Fig. 6c, bars 1 and 2). When comparing SCC tumors to normal skin, both pretreated with vehicle, a 2-fold increase was observed (Fig. 6c, compare bars 1 and 3), and the relative increase in PpIX was also significant when comparing the effect of VD upon PpIX production within the SCC tumors (~2-fold; Fig. 6c, compare bars 3 and 4). Overall, these data show that the PpIX-elevating effect of VD is specific to neoplastic (AK/SCC) tissue.

Validation of the noninvasive imaging results using Ex vivo analysis of PpIX in SCC tumor cryosections

Frozen sections from UV-induced SCC tumors (2–4 mm in diameter) that received either vehicle (Aq) or VD treatment for 3 days prior to ALA application (4 h) were examined by confocal microscopy to detect the effect of VD on ALA induced PpIX synthesis. In addition to a higher amount of PpIX overall, PpIX was observed in a greater proportion of cells in the VD preconditioned tumors (Fig. 7a). Quantification of fluorescence intensity, averaged over the entire tumor, revealed that VD pretreatment had significantly increased tumor-specific ALA-induced PpIX synthesis (by 16-fold) as compared to vehicle pretreatment alone (Fig. 7b).

DISCUSSION

In this study, we have demonstrated that optical imaging methods (wide-field camera-based and probe-based imaging systems) can semiquantitatively map the relative levels of PpIX generated in preneoplastic and neoplastic skin lesions, after application of ALA on the skin of mice. In addition, we have shown that the initial appearance and subsequent growth of SCC tumors can be followed precisely using the PpIX fluorescence detection capability of a multispectral imaging system, Maestro EX IVIS®. We also used these detection methodologies to investigate a potential SCC treatment technique, i.e., the combined use of Vitamin D and ALA-based PDT. Based on our *in vivo* PpIX fluorescence measurements (Fig. 5 and 6) and *ex vivo* tumor analysis data (Fig. 7), we showed that preconditioning of UV-induced AK/SCC tumors with VD prior to ALA application, triggers a significant increase in tumor-specific PpIX production. PpIX is not only a fluorescence emitter but also a photosensitizer, and the full photodynamic therapy regimen to treat the skin cancer (not done in this study) would be to apply very high-intensity light to activate the PpIX and kill

the tumor cells. Therefore, the application we have demonstrated may be best described as pre-treatment monitoring, which could be useful for predicting the responsiveness of tumors to PDT.

As reviewed recently (29), several researchers have developed wide-field camera based imaging (30–34) and fiber optic probe based point measurements (35–38) to investigate the pharmacokinetics of PpIX accumulation in skin tumors (39–42). Such methods have also been used to evaluate PDT treatment approaches (6, 43, 28). These spectral imaging methods (44–46) and fiber optic probes (47, 48) provided the global picture, or localized quantitative estimates of PpIX fluorescence, respectively. However, the spectral resolution in these previous approaches was not adequate to spectrally resolve the fluorescence collected at multiple wavelengths, to allow for decoupling of multiple sources of fluorescence within the tissue including the photosensitizer (e.g., PpIX), photoproducts, and tissue autofluorescence. The multispectral imaging system employed here, Maestro EX IVIS®, acquires fluorescence over a range of wavelengths, and can determine the extent of fluorophore accumulation by removing the autofluorescence (49). The excellent sensitivity and high signal-to-noise ratio of Maestro EX IVIS® has enabled us to calculate the pure PpIX spectrum (Fig. 2a) present in the mixed spectral image obtained 4 h post ALA application. The PpIX fluorescence measurements (Fig. 3d) detected by our own custom-built dosimeter system in the skin of UV exposed mice correlate very well with the optical mapping of PpIX in IVIS fluorescence images (Fig. 2f). Together, our data show that skin regions that have undergone field cancerization, can be delineated and differentiated from normal skin using optical imaging methods based upon PpIX fluorescence even when the developing tumors are too small to see visually.

One question to consider is whether the changes in PpIX accumulation observed here were influenced by UV- or VD-related changes in the stratum corneum that result in changes in topical ALA uptake. Chronic UV exposure of hairless mouse epidermis is known to cause thickening of the stratum corneum and impairment of barrier function (i.e., increased transepidermal water loss)(50). However, because these stratum corneum defects persist for months after UV is stopped (50), it seems unlikely that the broad areas of intense PpIX accumulation observed in our mice during UV exposure (see Fig. 4c, weeks 14–20) are due to increased stratum corneum permeability alone, because the PpIX signal rapidly diminished after UV cessation (Fig. 4c, weeks 21–24). Similarly, PpIX signals in AK/SCC-bearing skin, which were higher after VD-pretreatment than after vehicle-pretreatment alone (Fig. 5), cannot simply be attributed to increased ALA uptake in normal keratinoctyes because other published studies in several different tumor models, in which mice were preconditioned with VD (or vehicle) and treated with ALA for 4 h and then exposed to red light (PDT), showed negligible cell death in normal skin keratinocytes in either the absence or presence of VD (22, 23).

Although the optical imaging methods used in this study are sensitive enough to detect the increase in ALA induced PpIX synthesis caused by pretreatment with Vitamin D, the fold differences observed (Fig. 5 and Fig. 6) are much less than those observed in *ex vivo* analyses of biopsied tumors (Fig. 7). This is probably due to the relative inability of optical imaging techniques to excite PpIX (using surface illumination) and to collect the

fluorescence from PpIX molecules present deep in the skin as compared to the histology specimens. A tomographic approach to collect fluorescence light would seem a logical way to address this problem. However, scattering and diffusion of light within tissues represent a major barrier to obtaining high-resolution two-dimensional (2-D) fluorescent images. Some co-registration approaches have successfully coupled 2-D fluorescence tomography with techniques such as ultrasound (US) (51) and optical coherence tomography (OCT) (52–54) to allow quantification of fluorescence with high speed and sensitivity over a depth range of 2 mm (reviewed in Ref. (29)). Even so, these approaches use diffuse signals and provide a complex parametric representation of the sampled tissue volume. More recently, a dual channel red/blue fluorescence spectrometer-based point probe dosimeter system was developed to sample PpIX fluorescence from superficial and deeper tissue layers (28).

In conclusion, the optical imaging methods used here are noninvasive and can be used to provide an early visualization of SCC tumors, to monitor the tumor size, and to evaluate preconditioning regimens for enhancing PpIX concentrations. Additional studies are needed to develop calibration curves to measure the accurate concentration of PpIX present in the tumors, which could obviate the need for performing biopsies to predict treatment response. VD preconditioning was shown here to improve the PpIX synthesizing capability, with good tumor selectivity. Based upon these results, and building upon our previous studies that showed significant improvements in ALA-PDT mediated tumor cell death after a VD pretreatment of SCC tumors implanted subcutaneously in mice (21, 22), the time may be right for a pilot clinical trial to test the efficiency of this particular combination approach for early cutaneous SCC in humans.

Acknowledgments

We thank Dr. Vinod Labhasetwar (Lerner Research Institute, Cleveland Clinic) for offering the Maestro EX IVIS® instrument to use in our experiments, Dr. Judy Drazba (Lerner Research Institute, Cleveland Clinic) for help with digital imaging, and Dr. Tayyaba Hasan (Massachusetts General Hospital) for her continuing mentorship and support. This project was carried out with support from National Cancer Institute/NIH (Grant P01-CA84203, Dr. Tayyaba Hasan and Dr. Edward V. Maytin) and a *Dissertation Research Award* from Cleveland State University (Kishore R. Rollakanti).

References

1. Ratushny V, Gober MD, Hick R, Ridky TW, Seykora JT. From keratinocyte to cancer: the pathogenesis and modeling of cutaneous squamous cell carcinoma. J Clin Invest. 2012; 122:464–472. [PubMed: 22293185]
2. Kallini JR, Hamed N, Khachemoune A. Squamous cell carcinoma of the skin: epidemiology, classification, management, and novel trends. Int J Dermatol. 2015; 54:130–140. [PubMed: 25428226]
3. Miller DL, Weinstock MA. Nonmelanoma skin cancer in the United States: incidence. J Am Acad Dermatol. 1994; 30:774–778. [PubMed: 8176018]
4. Wolff, K.; Johnson, RA.; Fitzpatrick, TB. Fitzpatrick's Color Atlas and Synopsis of Clinical Dermatology. McGraw-Hill Medical; New York: 2009.
5. Stern RS, Study PFU. The risk of squamous cell and basal cell cancer associated with psoralen and ultraviolet A therapy: a 30-year prospective study. J Am Acad Dermatol. 2012; 66:553–562. [PubMed: 22264671]
6. Warren CB, Lohser S, Wene LC, Pogue BW, Bailin PL, Maytin EV. Noninvasive fluorescence monitoring of protoporphyrin IX production and clinical outcomes in actinic keratoses following

short-contact application of 5–aminolevulinate. J Biomed Opt. 2010; 15:051607. [PubMed: 21054081]

7. Piacquadio DJ, Chen DM, Farber HF, Fowler JF Jr, Glazer SD, Goodman JJ, Hruza LL, Jeffes EW, Ling MR, Phillips TJ, Rallis TM, Scher RK, Taylor CR, Weinstein GD. Photodynamic therapy with aminolevulinic acid topical solution and visible blue light in the treatment of multiple actinic keratoses of the face and scalp: investigator-blinded, phase 3, multicenter trials. Arch Dermatol. 2004; 140:41–46. [PubMed: 14732659]
8. Touma D, Yaar M, Whitehead S, Konnikov N, Gilchrest BA. A trial of short incubation, broad-area photodynamic therapy for facial actinic keratoses and diffuse photodamage. Arch Dermatol. 2004; 140:33–40. [PubMed: 14732657]
9. Szeimies RM, Karrer S, Radakovic-Fijan S, Tanew A, Calzavara-Pinton PG, Zane C, Sidoroff A, Hempel M, Ulrich J, Proebstle T, Meffert H, Mulder M, Salomon D, Dittmar HC, Bauer JW, Kernland K, Braathen L. Photodynamic therapy using topical methyl 5-aminolevulinate compared with cryotherapy for actinic keratosis: A prospective, randomized study. J Am Acad Dermatol. 2002; 47:258–262. [PubMed: 12140473]
10. Pariser DM, Lowe NJ, Stewart DM, Jarratt MT, Lucky AW, Pariser RJ, Yamauchi PS. Photodynamic therapy with topical methyl aminolevulinate for actinic keratosis: results of a prospective randomized multicenter trial. J Am Acad Dermatol. 2003; 48:227–232. [PubMed: 12582393]
11. Kennedy JC, Pottier RH. Endogenous protoporphyrin IX, a clinically useful photosensitizer for photodynamic therapy. J Photochem Photobiol B. 1992; 14:275–292. [PubMed: 1403373]
12. Hasan, T.; Ortel, B.; Solban, N.; Pogue, BW. Photodynamic therapy of cancer. In: Kufe, BRD.; Hait, W., et al., editors. Cancer Medicine. Decker, Inc; Hamilton, Ontario: 2006. p. 537-548.
13. Braathen LR, Szeimies RM, Basset-Seguin N, Bissonnette R, Foley P, Pariser D, Roelandts R, Wennberg AM, Morton CA. Guidelines on the use of photodynamic therapy for nonmelanoma skin cancer: an international consensus. International Society for Photodynamic Therapy in Dermatology, 2005. J Am Acad Dermatol. 2007; 56:125–143. [PubMed: 17190630]
14. Fink-Puches R, Soyer HP, Hofer A, Kerl H, Wolf P. Long-term follow-up and histological changes of superficial nonmelanoma skin cancers treated with topical delta-aminolevulinic acid photodynamic therapy. Arch Dermatol. 1998; 134:821–826. [PubMed: 9681345]
15. Campbell SM, Tyrrell J, Marshall R, Curnow A. Effect of MAL-photodynamic therapy on hypertrophic scarring. Photodiagnosis Photodyn Ther. 2010; 7:183–188. [PubMed: 20728843]
16. Karrer S, Bosserhoff AK, Weiderer P, Landthaler M, Szeimies RM. Influence of 5-aminolevulinic acid and red light on collagen metabolism of human dermal fibroblasts. J Invest Dermatol. 2003; 120:325–331. [PubMed: 12542540]
17. Anand S, Ortel BJ, Pereira SP, Hasan T, Maytin EV. Biomodulatory approaches to photodynamic therapy for solid tumors. Cancer Lett. 2012; 326:8–16. [PubMed: 22842096]
18. Sinha AK, Anand S, Ortel BJ, Chang Y, Mai Z, Hasan T, Maytin EV. Methotrexate used in combination with aminolaevulinic acid for photodynamic killing of prostate cancer cells. Br J Cancer. 2006; 95:485–495. [PubMed: 16868543]
19. Anand S, Honari G, Hasan T, Elson P, Maytin EV. Low-dose methotrexate enhances aminolevulinate-based photodynamic therapy in skin carcinoma cells in vitro and in vivo. Clin Cancer Res. 2009; 15:3333–3343. [PubMed: 19447864]
20. Maytin EV, Lohser S, Tellez A, Wene L, Ishak R, Anand S. Clinical studies of combined photodynamic therapy using 5-fluorouracil and methyl-aminolevulinate in patients at high risk for squamous cell carcinoma. Proceedings of the Proc SPIE. 2013; 8568
21. Anand S, Wilson C, Hasan T, Maytin EV. Vitamin D3 enhances the apoptotic response of epithelial tumors to aminolevulinate-based photodynamic therapy. Cancer Res. 2011; 71:6040–6050. [PubMed: 21807844]
22. Anand S, Rollakanti KR, Horst RL, Hasan T, Maytin EV. Combination of oral vitamin D3 with photodynamic therapy enhances tumor cell death in a murine model of cutaneous squamous cell carcinoma. Photochem Photobiol. 2014; 90:1126–1135. [PubMed: 24807677]
23. Rollakanti KR, Anand S, Maytin EV. Vitamin D enhances the efficacy of photodynamic therapy in a murine model of breast cancer. Cancer Med. 2015; 4:633–642. [PubMed: 25712788]

24. Rollakanti KR, Anand S, Maytin EV. Topical calcitriol prior to photodynamic therapy enhances treatment efficacy in non-melanoma skin cancer mouse models. Proc SPIE Int Soc Opt Eng. 2015 Mar 2.9308:93080Q.
25. Agarwal R, Athar M, Elmets CA, Bickers DR, Mukhtar H. Photodynamic therapy of chemically- and ultraviolet B radiation-induced murine skin papillomas by chloroaluminum phthalocyanine tetrasulfonate. Photochem Photobiol. 1992; 56:43–50. [PubMed: 1508981]
26. de Gruijl FR. Photocarcinogenesis: UVA vs. UVB radiation. Skin Pharmacol Appl Skin Physiol. 2002; 15:316–320. [PubMed: 12239425]
27. Feldman SR, Fleischer AB Jr. Progression of actinic keratosis to squamous cell carcinoma revisited: clinical and treatment implications. Cutis. 2011; 87:201–207. [PubMed: 21644496]
28. Kanick SC, Davis SC, Zhao Y, Hasan T, Maytin EV, Pogue BW, Chapman MS. Dual-channel red/blue fluorescence dosimetry with broadband reflectance spectroscopic correction measures protoporphyrin IX production during photodynamic therapy of actinic keratosis. J Biomed Opt. 2014; 19:75002. [PubMed: 24996661]
29. Rollakanti KR, Kanick SC, Davis SC, Pogue BW, Maytin EV. Techniques for fluorescence detection of protoporphyrin IX in skin cancers associated with photodynamic therapy. Photonics Lasers Med. 2013; 2:287–303. [PubMed: 25599015]
30. Ascencio M, Collinet P, Farine MO, Mordon S. Protoporphyrin IX fluorescence photobleaching is a useful tool to predict the response of rat ovarian cancer following hexaminolevulinate photodynamic therapy. Lasers Surg Med. 2008; 40:332–341. [PubMed: 18563777]
31. Heyerdahl H, Wang I, Liu DL, Berg R, Andersson-Engels S, Peng Q, Moan J, Svanberg S, Svanberg K. Pharmacokinetic studies on 5-aminolevulinic acid-induced protoporphyrin IX accumulation in tumours and normal tissues. Cancer Lett. 1997; 112:225–231. [PubMed: 9066732]
32. Pye A, Curnow A. Direct comparison of delta-aminolevulinic acid and methyl-aminolevulinate-derived protoporphyrin IX accumulations potentiated by desferrioxamine or the novel hydroxypyridinone iron chelator CP94 in cultured human cells. Photochem Photobiol. 2007; 83:766–773. [PubMed: 17576385]
33. Tyrrell J, Campbell SM, Curnow A. Monitoring the accumulation and dissipation of the photosensitizer protoporphyrin IX during standard dermatological methyl-aminolevulinate photodynamic therapy utilizing non-invasive fluorescence imaging and quantification. Photodiagnosis Photodyn Ther. 2011; 8:30–38. [PubMed: 21333932]
34. van der Beek N, de Leeuw J, Demmendal C, Bjerring P, Neumann HA. PpIX fluorescence combined with auto-fluorescence is more accurate than PpIX fluorescence alone in fluorescence detection of non-melanoma skin cancer: an intra-patient direct comparison study. Lasers Surg Med. 2012; 44:271–276. [PubMed: 22170313]
35. Wang I, Svanberg K, Andersson-Engels S, Berg R, Svanberg S. Photodynamic therapy of non-melanoma skin malignancies with topical δ-amino levulinic acid: diagnostic measurements. Proc SPIE Int Soc Opt Eng. 1995; 2371:243–252.
36. Johansson J, Berg R, Svanberg K, Svanberg S. Laser-induced fluorescence studies of normal and malignant tumour tissue of rat following intravenous injection of delta-amino levulinic acid. Lasers Surg Med. 1997; 20:272–279. [PubMed: 9138256]
37. Peng Q, Moan J, Warloe T, Nesland JM, Rimington C. Distribution and photosensitizing efficiency of porphyrins induced by application of exogenous 5-aminolevulinic acid in mice bearing mammary carcinoma. Int J Cancer. 1992; 52:433–443. [PubMed: 1399120]
38. Rhodes LE, Tsoukas MM, Anderson RR, Kollias N. Iontophoretic delivery of ALA provides a quantitative model for ALA pharmacokinetics and PpIX phototoxicity in human skin. J Invest Dermatol. 1997; 108:87–91. [PubMed: 8980294]
39. Smits T, Robles CA, van Erp PE, van de Kerkhof PC, Gerritsen MJ. Correlation between macroscopic fluorescence and protoporphyrin IX content in psoriasis and actinic keratosis following application of aminolevulinic acid. J Invest Dermatol. 2005; 125:833–839. [PubMed: 16185285]
40. Golub AL, Gudgin Dickson EF, Kennedy JC, Marcus SL, Park Y, Pottier RH. The Monitoring of ALA-Induced Protoporphyrin IX Accumulation and Clearance in Patients with Skin Lesions by In

Vivo Surface-Detected Fluorescence Spectroscopy. Lasers Med Sci. 1999; 14:112–122. [PubMed: 24519166]

41. Fritsch C, Lehmann P, Stahl W, Schulte KW, Blohm E, Lang K, Sies H, Ruzicka T. Optimum porphyrin accumulation in epithelial skin tumours and psoriatic lesions after topical application of delta-aminolaevulinic acid. Br J Cancer. 1999; 79:1603–1608. [PubMed: 10188913]
42. Rick K, Sroka R, Stepp H, Kriegmair M, Huber RM, Jacob K, Baumgartner R. Pharmacokinetics of 5-aminolevulinic acid-induced protoporphyrin IX in skin and blood. J Photochem Photobiol B. 1997; 40:313–319. [PubMed: 9372622]
43. Piffaretti F, Zellweger M, Kasraee B, Barge J, Salomon D, van den Bergh H, Wagnieres G. Correlation between protoporphyrin IX fluorescence intensity, photobleaching, pain and clinical outcome of actinic keratosis treated by photodynamic therapy. Dermatology. 2013; 227:214–225. [PubMed: 24135436]
44. Valdes PA, Leblond F, Kim A, Wilson BC, Paulsen KD, Roberts DW. A spectrally constrained dual-band normalization technique for protoporphyrin IX quantification in fluorescence-guided surgery. Opt Lett. 2012; 37:1817–1819. [PubMed: 22660039]
45. Saager RB, Cuccia DJ, Saggese S, Kelly KM, Durkin AJ. Quantitative fluorescence imaging of protoporphyrin IX through determination of tissue optical properties in the spatial frequency domain. J Biomed Opt. 2011; 16:126013. [PubMed: 22191930]
46. Sunar U, Rohrbach DJ, Morgan J, Zeitouni N, Henderson BW. Quantification of PpIX concentration in basal cell carcinoma and squamous cell carcinoma models using spatial frequency domain imaging. Biomed Opt Express. 2013; 4:531–537. [PubMed: 23577288]
47. Amelink A, Kruijt B, Robinson DJ, Sterenborg HJ. Quantitative fluorescence spectroscopy in turbid media using fluorescence differential path length spectroscopy. J Biomed Opt. 2008; 13:054051. [PubMed: 19021431]
48. Kanick SC, Robinson DJ, Sterenborg HJ, Amelink A. Extraction of intrinsic fluorescence from single fiber fluorescence measurements on a turbid medium. Opt Lett. 2012; 37:948–950. [PubMed: 22378448]
49. Jaffer H I, Adjei M, Labhasetwar V. Optical imaging to map blood-brain barrier leakage. Sci Rep. 2013; 3:3117. [PubMed: 24178124]
50. Kambayashi H, Odake Y, Takada K, Funasaka Y, Ichihashi M. Involvement of changes in stratum corneum keratin in wrinkle formation by chronic ultraviolet irradiation in hairless mice. Exp Dermatol. 2003; 12(Suppl 2):22–27. [PubMed: 14756520]
51. Zhu Q, Chen NG, Piao D, Guo P, Ding X. Design of near-infrared imaging probe with the assistance of ultrasound localization. Appl Opt. 2001; 40:3288–3303. [PubMed: 11958271]
52. Kepshire DS, Davis SC, Dehghani H, Paulsen KD, Pogue BW. Subsurface diffuse optical tomography can localize absorber and fluorescent objects but recovered image sensitivity is nonlinear with depth. Appl Opt. 2007; 46:1669–1678. [PubMed: 17356609]
53. Kepshire D, Davis SC, Dehghani H, Paulsen KD, Pogue BW. Fluorescence tomography characterization for sub-surface imaging with protoporphyrin IX. Opt Express. 2008; 16:8581–8593. [PubMed: 18545571]
54. Davis SC, Dehghani H, Wang J, Jiang S, Pogue BW, Paulsen KD. Image-guided diffuse optical fluorescence tomography implemented with Laplacian-type regularization. Opt Express. 2007; 15:4066–4082. [PubMed: 19532650]

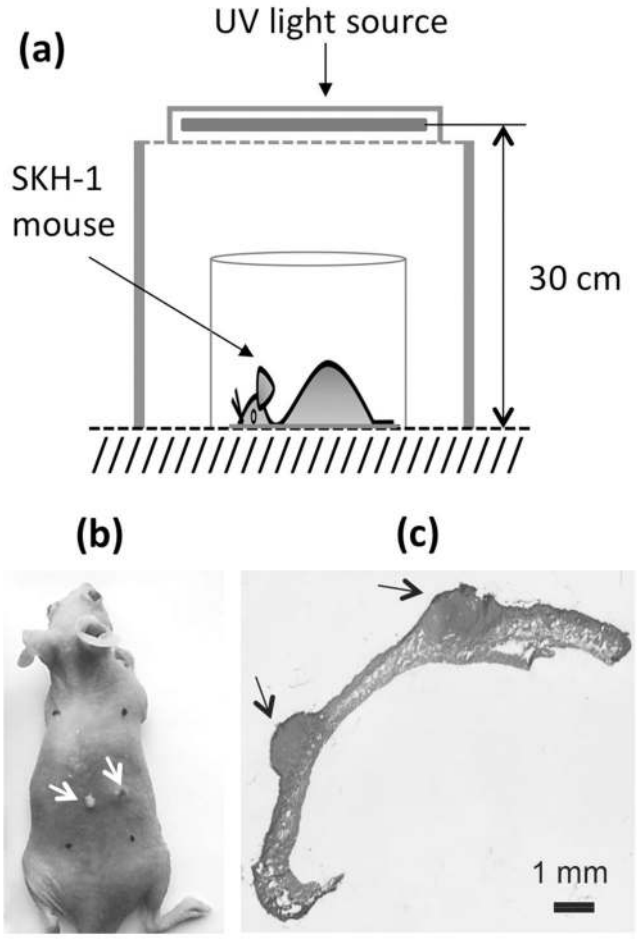

Fig. 1.

UV induced AK/SCC mouse model. (a) Set up of ultraviolet (UV) light bulbs for chronic exposure of SKH-1 mice. (b) Photograph of hairless SKH-1 mouse; arrows point to AK/SCC tumors on the UV-exposed back of the animal. (c) H&E stained SCC tumors (arrow), and adjacent skin. Scale bar, 1 mm.

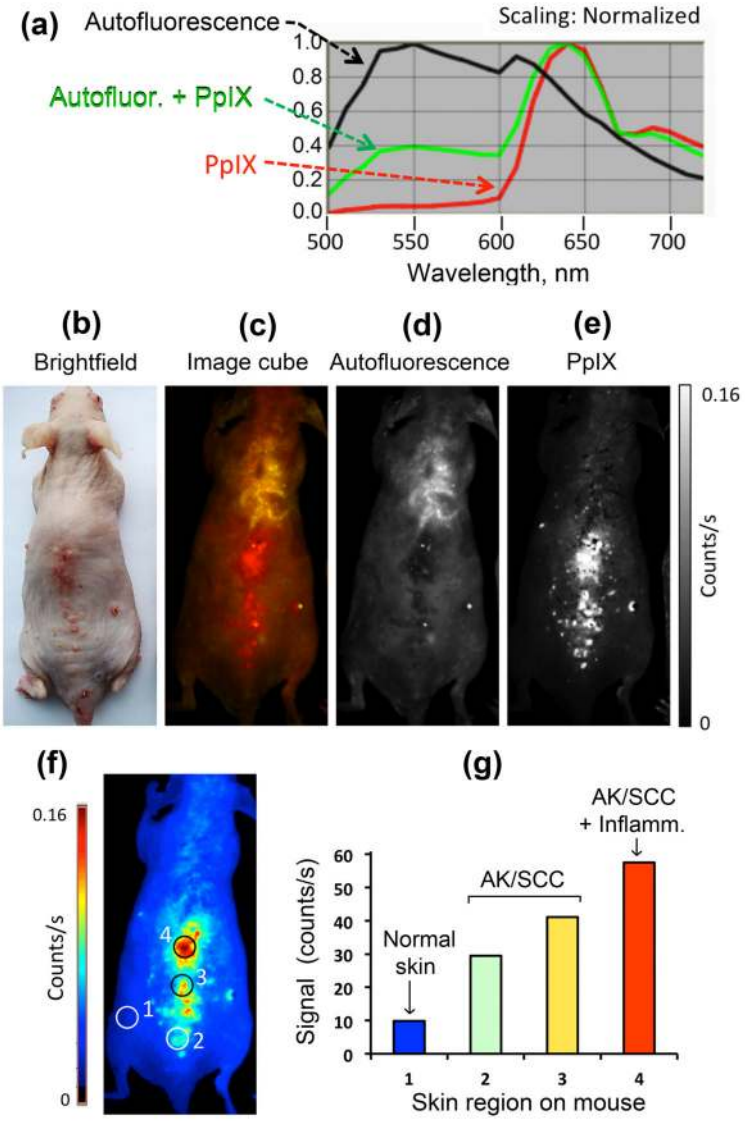

Fig. 2.

Quantification of optical signals from PpIX fluorescence measured in an AK/SCC-bearing mouse using Maestro EX IVIS®. (a) Pure PpIX spectrum (red line), calculated using Maestro EX 3.0 software by subtracting autofluorescence from the mixed spectrum (Autofl. +PpIX) obtained before and 4 h after ALA application, respectively. (b) Brightfield image of a tumor-bearing mouse obtained using an 8.1 MP SONY camera. (c) Image cube acquired from the mouse using the Maestro EX IVIS® blue filter set (λ_{ex}: 455 nm; λ_{em}: 490 – 720 nm). (d) Autofluorescence. (e) PpIX signal, separated using the calculated spectra. (f) Rainbow display image of the mouse showing the PpIX signal distribution. (g) Quantification of optical signal intensity, in regions (indicated by different colors) that correspond to distinct histological characteristics, ranging from normal, preneoplastic/ neoplastic (AK/SCC), and neoplastic with inflammation (SCC + Inflamm).

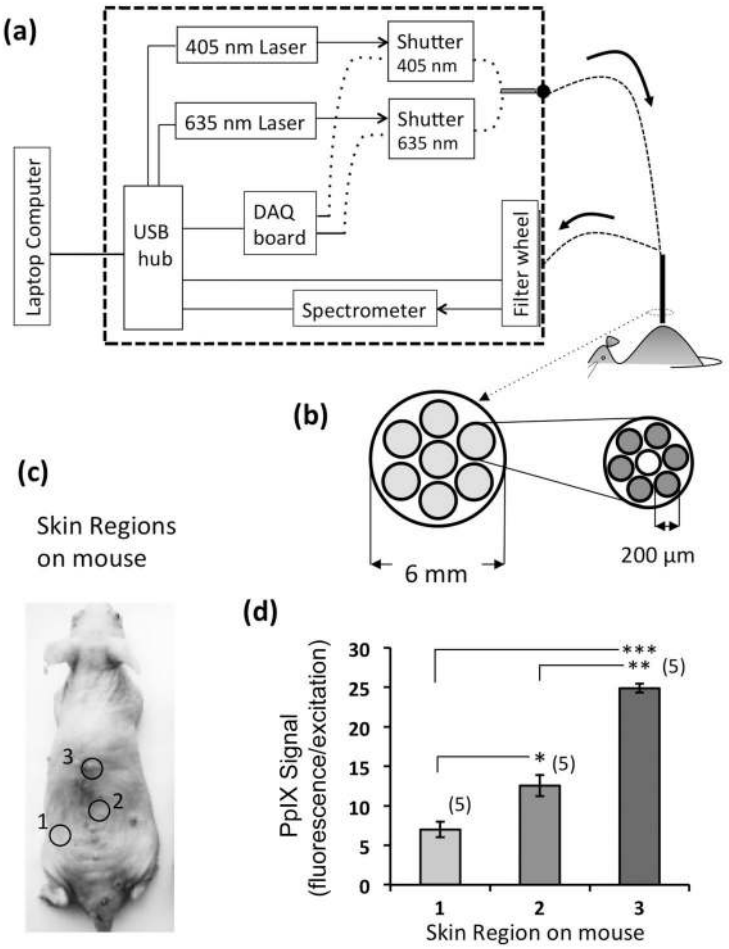

Fig. 3.

Quantification of PpIX fluorescence in AK/SCC mouse (4 h post ALA) with our probe based dosimeter system. (a) Schematic of the dosimeter setup, showing different system components and their arrangement in a chassis. Outgoing and incoming dotted lines (curved arrows) represent the pathway for excitation and emission (PpIX fluorescence), respectively. (b) Arrangement of optical fibers in the probe tip. Within each of 7 identical bundles in the 6 mm diameter array (*light gray*), the following fiber arrangement is found. A 200 µm diameter source fiber in the center (*white*) is used to excite PpIX, and surrounding this are six similar fibers (*black*) which transmit light remitted from the tissue back through the filter wheel and into the spectrometer. (c) Brightfield image of UV-exposed SCC mouse with three circles representing three different regions (1- minimal UV exposure; 2- AK/SCC with no inflammation; 3- AK/SCC with inflammation, judged by erythema); and (d) their corresponding PpIX signal quantification. Data are shown as Mean ±SEM, n=5 mice. *p = 0.01, 1 vs. 2; **p = 0.0003, 2 vs. 3; ***p = 0.000003, 1 vs. 3.

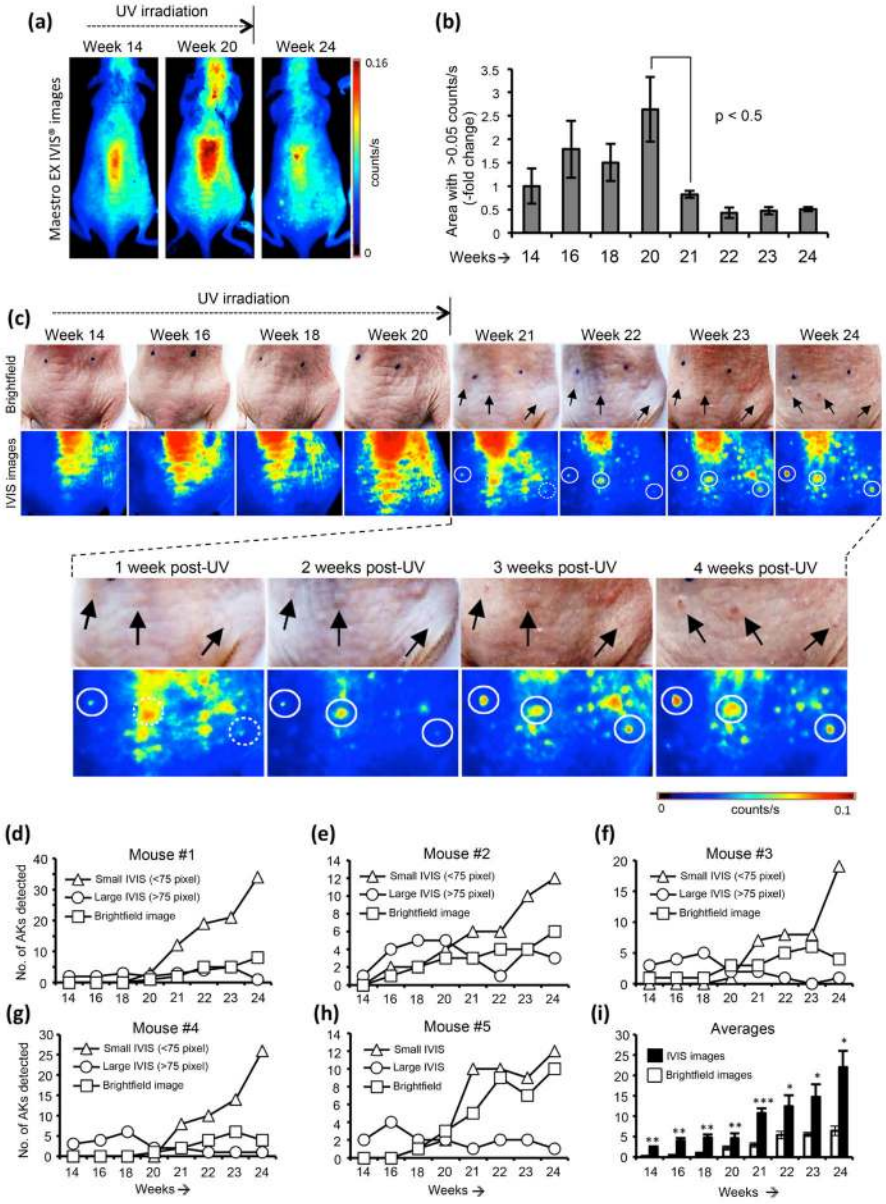

Fig. 4.

Non-invasive monitoring of AK/SCC development in SKH-1 mice during a 24-week UV carcinogenesis protocol, using Maestro EX IVIS®. (a) Examples of images of PpIX fluorescence intensity (at 4 h post ALA) obtained with Maestro EX IVIS®. (b) Quantification of PpIX showing relative changes in the area of skin emitting >0.05 counts/s of fluorescence between week 14 and week 24. Mean ± SEM, n=4 mice. (c) Brightfield images on the lower back of a mouse from week 14 to 24, and the corresponding Maestro EX IVIS® images. In the enlargement, the visual appearance of AK lesions (*arrows* in top panels) and the fluorescence signal at corresponding locations (*circles* in bottom panels) can be compared. (d–h) Line plots of 5 mice showing the number of AKs detectable from Maestro EX IVIS® and brightfield images. Inflammatory regions (>75 pixels) and AK

lesions (<75 pixels) were quantitated separately in IVIS images. (i) Quantification of AK lesions detected from brightfield images and IVIS images. Mean ± SEM, n=5 mice. *p < 0.05; **p = 0.003; ***p = 0.0007 (statistical significance over their corresponding brightfield image data).

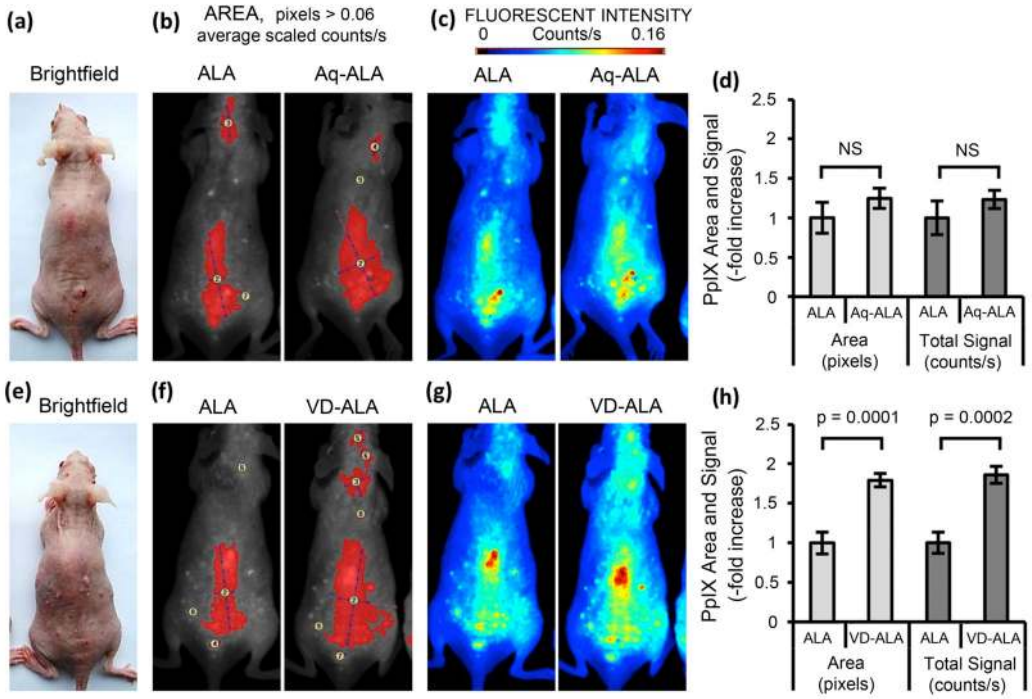

Fig. 5.

Vitamin D pretreatment enhances ALA-induced PpIX synthesis in AK/SCC tumors, as shown by Maestro EX IVIS®. Experiments were conducted using two groups of tumor-bearing mice (4 mice each), either pretreated with vehicle only (Aq; top row) or with Vitamin D ointment (VD; bottom row); see text for more details. Images show one example from each group of mice on the final day, after ALA was applied for 4 h and the images taken. (a, e) Visual appearance (brightfield images) of the mice; (b, f) Area overlay, outlining in red all pixels with >0.06 average scaled counts/s; (c, g) Optical images showing PpIX fluorescent signal intensity, with calibration scale shown at the top. (d, h) Quantification from all mice (each bar represents mean ± SEM, n=4); Each graph shows relative changes in the area overlay (first 2 bars), and in the fluorescent signal intensity (last 2 bars). Statistical significance between conditions was determined by unpaired 2-sided t-test. NS, not significant.

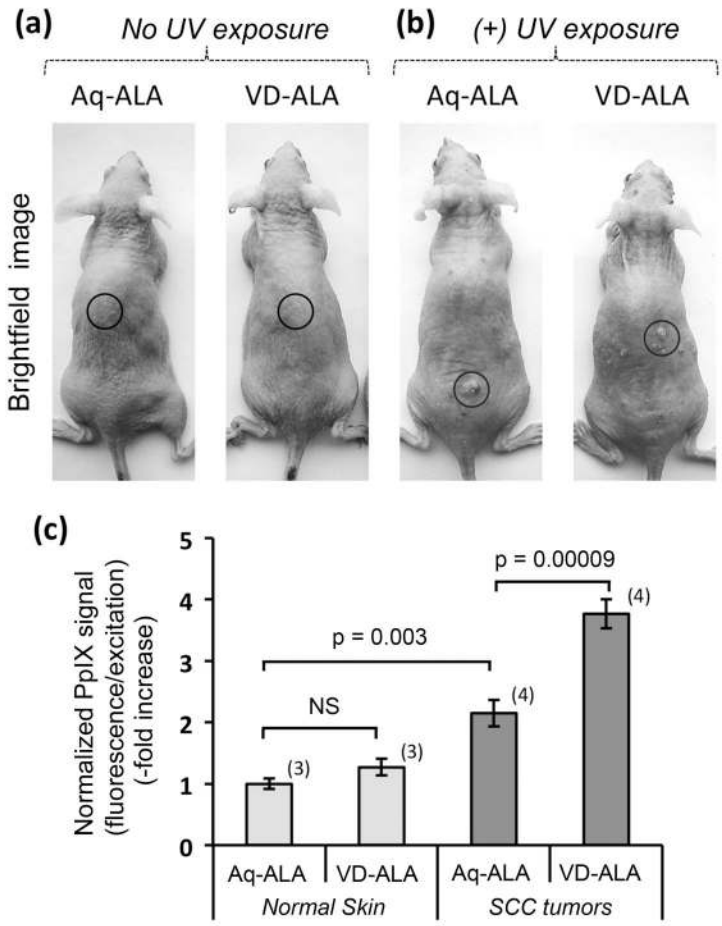

Fig. 6.

Vitamin D-mediated enhancement of ALA-induced PpIX accumulation occurs selectively in SCC tumors (and not in normal skin), as shown using the probe dosimeter system. Representative brightfield images of (a) control mice with no UV exposure, and (b) UV induced SCC mice that underwent UV exposure to induce AK/SCC lesions. In both cases, some mice received 3 days of Aquaphor pretreatment (Aq, left mouse) or Vitamin D pretreatment (VD, right mouse). Circles on the mice represent the regions used to measure PpIX fluorescence with the dosimeter. (c) Quantification of PpIX fluorescence from normal skin (Aq vs. VD pre-conditioning) and SCC tumors (Aq vs. VD preconditioning). Mean ± SEM, n=3–4 mice; data are fold increases relative to Aquaphor-normal skin controls. *P* values were calculated from unpaired 2-sided *t*-tests.

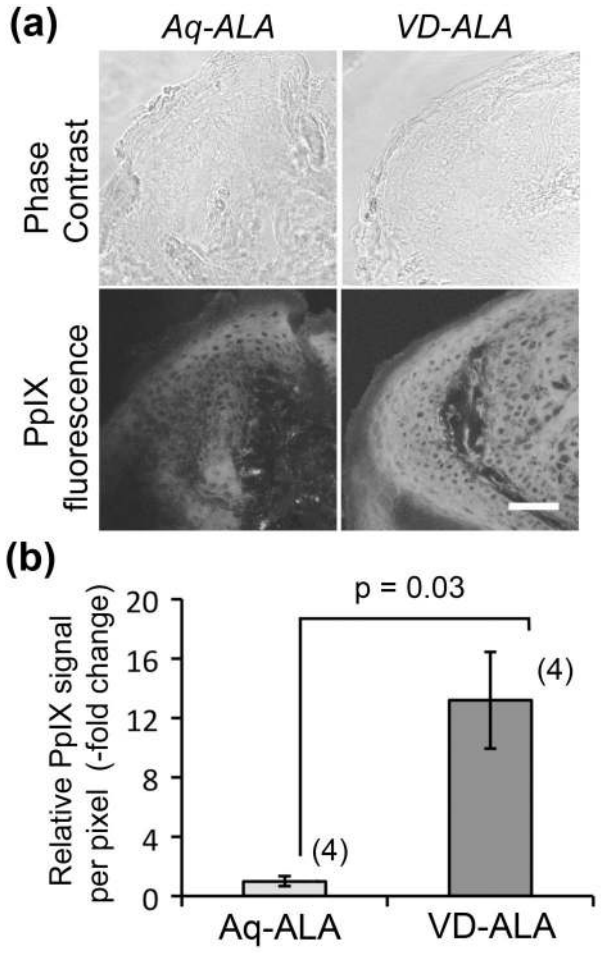

Fig. 7.

Ex vivo analysis of PpIX using confocal microscopy, as an independent method to verify VD-mediated enhancement of PpIX in SCC tumors. (a) Phase contrast (upper panels), and fluorescence images (lower panels) showing PpIX levels in tumor sections after 3 days of Aquaphor (Aq) or Vitamin D (VD) treatment followed by 4 h of ALA. Scale bar 50 μm. (b) Digital quantification of relative PpIX levels (fold change), using IPLab software; Mean ± SEM of three representative images from each of 4 tumors per treatment condition. *P* values was calculated from unpaired 2-sided *t*-tests.